Arch Appl Mech (2011) 81: 1307–1322
DOI 10.1007/s00419-010-0488-6

ORIGINAL

M. R. Karamooz Ravari · M. R. Forouzan

Frequency equations for the in-plane vibration of orthotropic circular annular plate

Received: 11 May 2010 / Accepted: 11 November 2010 / Published online: 24 November 2010

Abstract Orthotropic circular annular plates have a lot of applications in engineering such as space structures and rotary machines. In this paper, frequency equations for the in-plane vibration of the orthotropic circular annular plate for general boundary conditions were derived. To obtain the frequency equation, first the equation of motion for the circular annular plate in the cylindrical coordinate is derived by using the stress-strain-displacement expressions. Helmholtz decomposition is used to uncouple the equations of motion. The wave equation is obtained by assumption a harmonic solution for the uncoupled equations. Using the separation of the variables leads to the general wave equation solution and the in-plane displacements in the r and θ directions. Finally, boundary conditions are exerted and the natural frequency is derived for general boundary conditions. The obtained results are validated by comparing with the previously reported and those from finite element analysis.

Keywords In-plane · Vibration · Orthotropic material · Frequency equation · General boundary condition

List of symbols

R	Outer radius
R_0	Inner radius
ξ	Dimensionless coordinates r/R
η	Radius ratio R_0/R
ρ	Density
E_r, E_θ	Youngs moduli related to the r and θ directions, respectively
ν_r, ν_θ	Poisson ratios related to r and θ directions, respectively
G	Modulus of elasticity in shear
b	Stiffness ratio E_θ/E_r
g	Dimensionless shear modulus defined in text
t	Time
σ_r, σ_θ	Normal stress in r and θ direction respectively
$\tau_{r\theta}$	shear stress
ε_r, ε_θ	Normal strain in r and θ direction respectively
$\gamma_{r\theta}$	Shear strain
u, v	Displacements in r and θ directions, respectively
φ, $\mathbf{H}$	Scalar and vector potentials
Ω	Non-dimensional natural frequencies defined in text
∇	Gradient operator

M. R. Karamooz Ravari (✉) · M. R. Forouzan
Department of Mechanical Engineering, Isfahan University of Technology,
84156-83111 Isfahan, Iran
E-mail: m.karamoozravari@me.iut.ac.ir
Tel.: +989132960234

1 Introduction

Circular annular plates have a wide usage in engineering applications such as space structures, electronic components and rotating machinery. Despite the information about out-of-plane vibration of plates is wide, the studies which reported on the in-plane vibration of circular annular plates are little.

Obtaining the frequency of circular annular disks has been treated in a few studies. Irie et al. [1] used transfer matrix formulation to examine the in-plane vibrations of circular and annular disks. Natural frequencies were obtained for several radius ratios of annular disks with combinations of free and clamped boundary conditions at the inner and outer edges but mode shapes were not presented. Ambati et al. [2] studied in-plane vibrations of solid disks and rings. The natural frequencies and mode shapes were evaluated for general case of annular configuration as hole sizes increased from thin disks to narrow thin rings. Obtained results were validated by experiments. Farag and Pan [3] analyzed the modal characteristics of in-plane vibrations of a solid disk with clamped outer edge. These studies were carried out for a limited set of boundary conditions. Holland [4] studied the free in-plane vibration of circular disks with free edges and presented frequency parameters for different values of Poisson's ratio by using trigonometric and Bessel functions. Kane and Mindlin [5] investigated the coupling between extensional vibration and the first mode of thickness vibration on the circular disk. Chen and Liu [6] studied the free in-plane vibration for various shapes of thin plates with a free edge, including a circular plate, and compared the nodal patterns of plates with different shapes. Love [7] solved the extensional vibration of an infinitely isotropic thin circular plate with free edge as an initial approach to the in-plane vibration of plates. Bashmal [8] et al. investigated a generalized formulation for the in-plane modal characteristics of circular annular disks under combinations of all possible classical boundary conditions for isotropic materials by Rayleigh–Ritz method. Chen and Jhu [9] investigated the effects of the clamping ratio on the critical speeds and the natural frequencies of the in-plane vibration of a spinning annular disk. Chan [10] derived the frequency equation for the in-plane vibration of the clamped circular disk of uniform thickness with an isotropic material in the elastic range by using Hamilton's principle and Helmholtz decomposition.

The main goal of the present paper is to obtain the in-plane frequency equation for the orthotropic circular annular plate under general boundary conditions.

2 Analysis

The present study analyzes a circular annular plate with external radius R and internal radius R_0 which lies in the $r - \theta$ plane, as shown in Fig. 1. The circular annular plate with an orthotropic material and uniform thickness is treated at the elastic range.

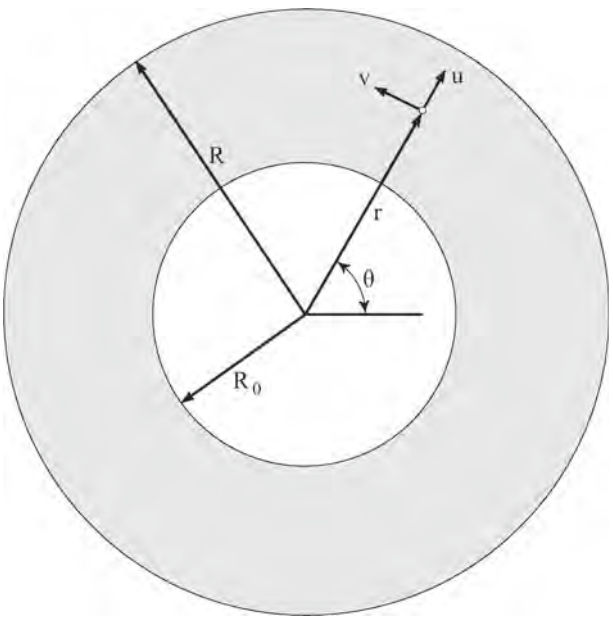

Fig. 1 A circular annular plate in cylindrical coordinate

2.1 Development of equations of motion for in-plane vibration

Using the coordinate system of Fig. 1 and the list of symbols as in the nomenclature, the basic equations of motion are written as [11]:

$$\frac{\partial \sigma_r}{\partial r} + \frac{\partial \tau_{r\theta}}{\partial \theta} + \frac{\sigma_r - \sigma_\theta}{r} = \rho \ddot{u} \tag{1}$$

And

$$\frac{\partial \tau_{r\theta}}{\partial r} + \frac{1}{r}\frac{\partial \sigma_\theta}{\partial \theta} + 2\frac{\tau_{r\theta}}{r} = \rho \ddot{v} \tag{2}$$

The stress–strain relationships for the orthotropic in-plane circular plate are as follow [12]:

$$\sigma_r = \frac{E_r}{1 - \nu_r \nu_\theta}(\varepsilon_r + \nu_\theta \varepsilon_\theta) \tag{3a}$$

$$\sigma_\theta = \frac{E_\theta}{1 - \nu_r \nu_\theta}(\varepsilon_\theta + \nu_r \varepsilon_r) \tag{3b}$$

While the shear stress–displacement relationship is:

$$\tau_{r\theta} = G\gamma_{r\theta} \tag{3c}$$

Also the strain–displacement relationships are reviewed in Ref. [8], for example, and are as follow:

$$\varepsilon_r = \frac{\partial u}{\partial r} \tag{4a}$$

$$\varepsilon_\theta = \frac{1}{r}\left(u + \frac{\partial v}{\partial \theta}\right) \tag{4b}$$

$$\gamma_{r\theta} = \frac{1}{r}\frac{\partial u}{\partial \theta} + \frac{\partial v}{\partial r} - \frac{v}{r} \tag{4c}$$

By substituting Eqs. 4 and 3 in Eqs. 1 and 2 and using of the Betti principle ($E_r \nu_\theta = E_\theta \nu_r$), equations of motion is expressed in terms of the displacement as:

$$\frac{E_r}{1 - \nu_r \nu_\theta}\left(\frac{\partial^2 u}{\partial r^2} + \frac{\nu_\theta}{r}\frac{\partial^2 v}{\partial r \partial \theta} + \frac{1}{r}\frac{\partial u}{\partial r}\right) - \frac{E_\theta}{1 - \nu_r \nu_\theta}\left(\frac{1}{r^2}\frac{\partial v}{\partial \theta} + \frac{u}{r^2}\right) + G\left(\frac{1}{r}\frac{\partial^2 v}{\partial r \partial \theta} + \frac{1}{r^2}\frac{\partial^2 u}{\partial \theta^2} - \frac{1}{r^2}\frac{\partial v}{\partial \theta}\right) = \rho \ddot{u} \tag{5}$$

$$\frac{E_\theta}{1 - \nu_r \nu_\theta}\left(\frac{1}{r^2}\frac{\partial^2 v}{\partial \theta^2} + \frac{1}{r^2}\frac{\partial u}{\partial \theta} + \frac{\nu_r}{r}\frac{\partial^2 u}{\partial r \partial \theta}\right) + G\left(\frac{\partial^2 v}{\partial r^2} + \frac{1}{r}\frac{\partial^2 u}{\partial r \partial \theta} + \frac{1}{r^2}\frac{\partial u}{\partial \theta} + \frac{1}{r}\frac{\partial v}{\partial r} - \frac{v}{r^2}\right) = \rho \ddot{v} \tag{6}$$

2.2 Frequency equation for in-plane vibration

The previously derived equations of motion are highly complex and coupled. However, a simpler set of equations can be obtained by introducing scalar and vector potentials φ and $\mathbf{H}$, known as the Helmholtz decomposition, such that [13,14]:

$$\mathbf{u} = \nabla \varphi + \nabla \times \mathbf{H} \tag{7}$$

Therefore, the scalar components of the in-plane displacement vector $\mathbf{u}$ in the cylindrical coordinate with $\frac{\partial}{\partial z} = 0$ can be expressed in the r and θ directions as [11,14]:

$$u = \frac{\partial \varphi}{\partial r} + \frac{1}{r}\frac{\partial H_z}{\partial \theta} \tag{8a}$$

$$v = \frac{1}{r}\frac{\partial \varphi}{\partial \theta} - \frac{\partial H_z}{\partial r} \tag{8b}$$

Substituting u and v from Eq. 8 in Eqs. 5 and 6 leads to two sets of differential equations:

$$(1-\nu_\theta-g)\frac{\partial^2 H_z}{\partial r^2}+\frac{b+g-1}{r}\frac{\partial H_z}{\partial r}+\frac{1-b}{r^2}H_z+\frac{g}{r^2}\frac{\partial^2 H_z}{\partial \theta^2}=\rho\frac{(1-\nu_r\nu_\theta)}{E_r}\ddot{H}_z \tag{9}$$

$$\frac{b}{r^2}\frac{\partial^2\varphi}{\partial\theta^2}+\frac{1}{r}\frac{\partial\varphi}{\partial r}+(b\nu_r+2g)\frac{\partial^2\varphi}{\partial r^2}=\rho\frac{(1-\nu_r\nu_\theta)}{E_r}\ddot{\varphi} \tag{10}$$

where $b=\frac{E_\theta}{E_r}$ and $g=G\frac{1-\nu_r\nu_\theta}{E_r}$.

To solve Eqs. 9 and 10, the solution assumes to be $H_z=\widehat{H}(r,\theta)e^{i\omega t}$ and $\varphi=\widehat{\varphi}(r,\theta)e^{i\omega t}$ then we have:

$$(1-\nu_\theta-g)\frac{\partial^2\widehat{H}}{\partial r^2}+\frac{b+g-1}{r}\frac{\partial\widehat{H}}{\partial r}+\frac{1-b}{r^2}\widehat{H}+\frac{g}{r^2}\frac{\partial^2\widehat{H}}{\partial\theta^2}=-\rho\frac{1-\nu_r\nu_\theta}{E_r}\omega^2\widehat{H} \tag{11}$$

$$\frac{b}{r^2}\frac{\partial^2\widehat{\varphi}}{\partial\theta^2}+\frac{1}{r}\frac{\partial\widehat{\varphi}}{\partial r}+(b\nu_r+2g)\frac{\partial^2\widehat{\varphi}}{\partial r^2}=-\rho\frac{1-\nu_r\nu_\theta}{E_r}\omega^2\widehat{\varphi} \tag{12}$$

By defining $\xi=\frac{r}{R}$, above equations can be modified as:

$$(1-\nu_\theta-g)\frac{\partial^2\widehat{H}}{\partial\xi^2}+\frac{b+g-1}{\xi}\frac{\partial\widehat{H}}{\partial\xi}+\frac{1-b}{\xi^2}\widehat{H}+\frac{g}{\xi^2}\frac{\partial^2\widehat{H}}{\partial\theta^2}=-\Omega^2\widehat{H} \tag{13}$$

$$\frac{b}{\xi^2}\frac{\partial^2\widehat{\varphi}}{\partial\theta^2}+\frac{1}{\xi}\frac{\partial\widehat{\varphi}}{\partial\xi}+(b\nu_r+2g)\frac{\partial^2\widehat{\varphi}}{\partial\xi^2}=-\Omega^2\widehat{\varphi} \tag{14}$$

where $\Omega^2=\rho\frac{1-\nu_r\nu_\theta}{E_r}R^2\omega^2$.

Application of the separation of the variable as $\widehat{H}=F(\xi)T(\theta)$ to Eq. 13 leads to:

$$(1-\nu_\theta-g)F''T+\frac{b+g-1}{\xi}F'T+\frac{1-b}{\xi^2}FT+\frac{g}{\xi^2}FT''=-\Omega^2FT \tag{15}$$

Equation 15 leads:

$$\frac{1-\nu_\theta-g}{g}\xi^2\frac{F''}{F}+\frac{b+g-1}{g}\xi\frac{F'}{F}+\left(\frac{1-b}{g}+\frac{\Omega^2\xi^2}{g}\right)=-\frac{T''}{T}=n^2 \tag{16}$$

In the above equation, the solutions for T are given by:

$$T(\theta)=\sin(n\theta) \tag{17}$$

Equation 16 leads to the following deferential equation for F:

$$\mu\xi^2F''+\lambda\xi F'+\left(\left(\frac{\Omega}{\sqrt{g}}\right)^2\xi^2-\alpha^2\right)F=0 \tag{18}$$

where $\mu=\frac{1-\nu_\theta-g}{g}$, $\lambda=\frac{b+g-1}{g}$ and $\alpha^2=n^2-\frac{1-b}{g}$.

The solution for F is obtained by:

$$F(\xi)=d_1\xi^{\frac{\mu-\lambda}{2\mu}}J_z\left(\frac{\Omega\xi}{\sqrt{\mu\sqrt{g}}}\right)+d_2\xi^{\frac{\mu-\lambda}{2\mu}}Y_z\left(\frac{\Omega\xi}{\sqrt{\mu\sqrt{g}}}\right) \tag{19}$$

where $z=\frac{\sqrt{\mu^2+(4\alpha^2-2\lambda)\mu+\lambda^2}}{2\mu}$ and J_z and Y_z are Bessel functions of first and second kind, respectively.

The separation of the variable as $\widehat{\varphi}=P(\xi)Q(\theta)$ yields $Q(\theta)=\cos(\theta)$ and the solution for P is also given by:

$$P(\xi)=c_1\xi^{\frac{\beta-1}{2\beta}}J_m\left(\frac{\Omega\xi}{\sqrt{\beta}}\right)+c_2\xi^{\frac{\beta-1}{2\beta}}Y_m\left(\frac{\Omega\xi}{\sqrt{\beta}}\right) \tag{20}$$

where $\beta=\frac{b\nu_\theta+2g}{g}$ and $m=\frac{\sqrt{\beta^2+(4n^2-2)\beta+4}}{2\beta}$.

Table 1 General boundary conditions applied to circular annular plate

Clamped-clamped	$u = 0, v = 0 \ @ \ \xi = \eta$ and $\xi = 1$
Clamped-free	$u = 0, v = 0 \ @ \ \xi = \eta$ and $\sigma_r = \sigma_\theta = 0 \ @ \ \xi = 1$
Free-clamped	$\sigma_r = \sigma_\theta = 0 \ @ \ \xi = \eta$ and $u = 0, v = 0 \ @ \ \xi = 1$
Free-free	$\sigma_r = \sigma_\theta = 0 \ @ \ \xi = \eta$ and $\sigma_r = \sigma_\theta = 0 \ @ \ \xi = 1$

Table 2 Non-dimensional first natural frequencies (Ω) of in-plane vibration for clamped conditions and isotropic material with $\nu = 0.3$

Radial ratio	Present study	Ref. [1]	Ref. [8]	Present study	Ref. [1]	Ref. [8]
	$n = 1$			$n = 2$		
0	2.092	1.985		3.157	3.046	
0.2	2.886	2.783	2.806	3.483	3.378	3.394
0.4	3.532	3.429	3.465	4.130	4.023	4.046
0.6	4.939	4.835		5.339	5.237	
0.8	9.476	9.370		9.658	9.547	
	$n = 3$			$n = 4$		
0	4.021	3.964		4.891	4.777	
0.2	4.119	4.066	4.084	4.916	4.802	4.811
0.4	4.766	4.707	4.737	5.470	5.287	5.360
0.6	5.893	5.832		6.650	6.541	
0.8	9.898	9.835		10.432	10.223	

Table 3 Non-dimensional first natural frequencies (Ω) of in-plane vibration for clamped-free boundary condition and isotropic material with $\nu = 0.3$

Radial ratio	Present study	Ref. [8]	Present study	Ref. [8]	Present study	Ref. [8]	Present study	Ref. [8]
	$n = 1$		$n = 2$		$n = 3$		$n = 4$	
0.2	0.928	0.919	1.548	1.542	2.163	2.157	2.781	2.779
0.4	1.297	1.281	1.969	1.965	2.469	2.463	2.926	2.924

Table 4 Non-dimensional first natural frequencies (Ω) of in-plane vibration for Free-clamped boundary condition and isotropic material with $\nu = 0.3$

Radial ratio	Present study	Ref. [8]	Present study	Ref. [8]	Present study	Ref. [8]	Present study	Ref. [8]
	$n = 1$		$n = 2$		$n = 3$		$n = 4$	
0.2	2.107	2.106	2.561	2.556	3.700	3.693	4.721	4.718
0.4	2.601	2.522	2.739	2.734	4.812	4.808	3.961	3.960

Table 5 Non-dimensional first natural frequencies (Ω) of in-plane vibration for Free-free boundary condition and isotropic material with $\nu = 0.3$

Radial ratio	Present study	Ref. [8]	Present study	Ref. [8]	Present study	Ref. [8]	Present study	Ref. [8]
	$n = 1$		$n = 2$		$n = 3$		$n = 4$	
0.2	1.661	1.651	1.120	1.111	2.074	2.072	2.768	2.766
0.4	1.700	1.682	0.727	0.721	1.623	1.619	2.485	2.482

The solutions for $\widehat{H}$ and $\widehat{\varphi}$ are obtained as:

$$\widehat{H}(\xi,\theta) = \left[d_1 \xi^{\frac{\mu-\lambda}{2\mu}} J_z\left(\frac{\Omega\xi}{\sqrt{\mu\sqrt{g}}}\right) + d_2 \xi^{\frac{\mu-\lambda}{2\mu}} Y_z\left(\frac{\Omega\xi}{\sqrt{\mu\sqrt{g}}}\right)\right] \sin(n\theta) \tag{21}$$

$$\widehat{\varphi}(\xi,\theta) = \left[c_1 \xi^{\frac{\beta-1}{2\beta}} J_m\left(\frac{\Omega\xi}{\sqrt{\beta}}\right) + c_2 \xi^{\frac{\beta-1}{2\beta}} Y_m\left(\frac{\Omega\xi}{\sqrt{\beta}}\right)\right] \cos(n\theta) \tag{22}$$

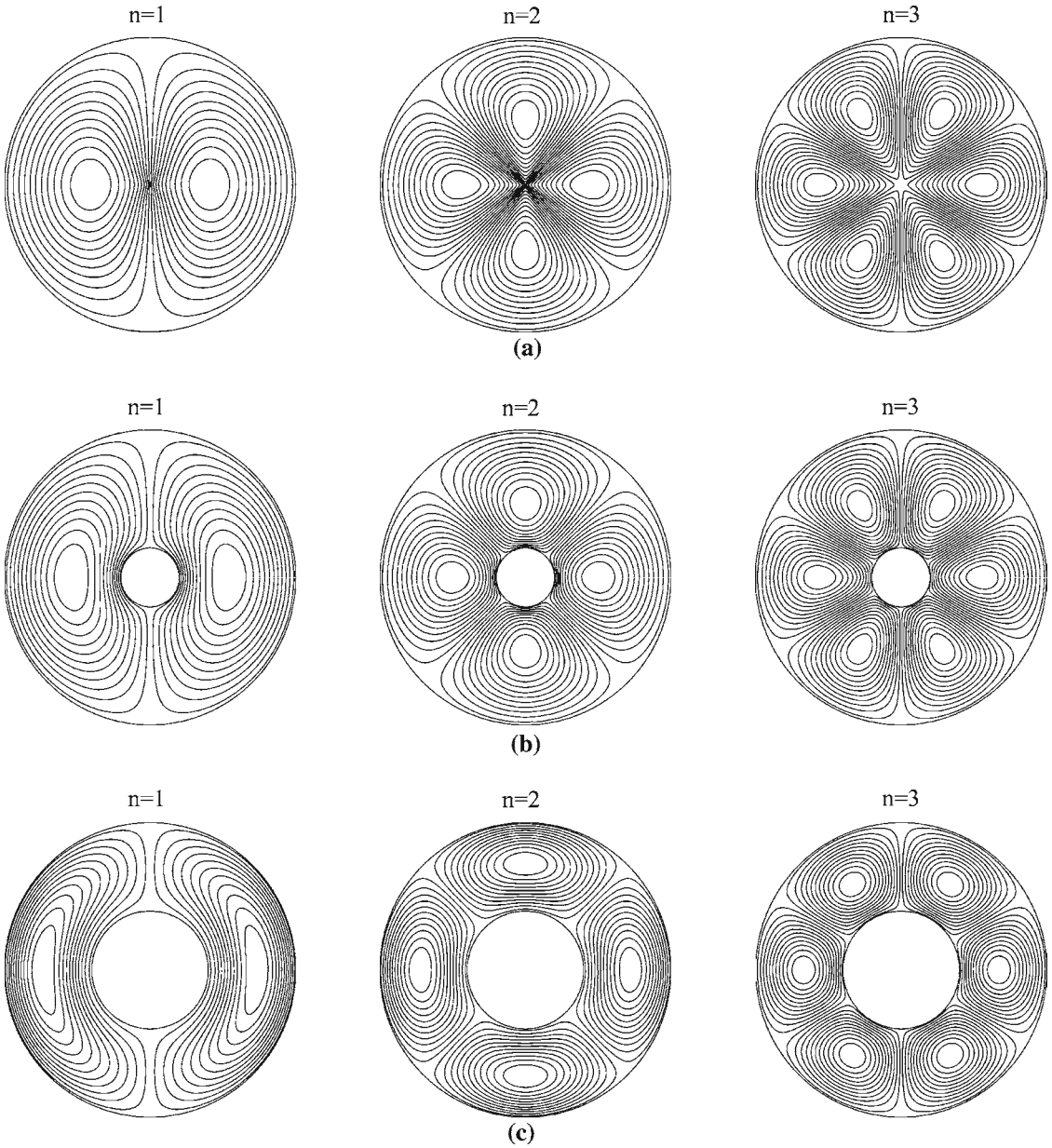

Fig. 2 Radial mode shapes distribution of Clamped-clamped boundary condition for n = 1, 2, 3 and **a** $\eta = 0$, **b** $\eta = 0.2$, **c** $\eta = 0.4$ corresponding to Table 2

Then, the displacements for $u = \widehat{u}e^{i\omega t}$ and $v = \widehat{v}e^{i\omega t}$ are given by:

$$\widehat{u} = \frac{1}{R}\left(\frac{\partial\widehat{\varphi}}{\partial\xi} + \frac{1}{\xi}\frac{\partial\widehat{H}}{\partial\theta}\right) = \frac{1}{R}\left(P' + \frac{n}{\xi}F\right)\cos(n\theta) \tag{23}$$

$$\widehat{v} = \frac{1}{R}\left(\frac{1}{\xi}\frac{\partial\widehat{\varphi}}{\partial\theta} - \frac{\partial\widehat{H}}{\partial\xi}\right) = \frac{1}{R}\left(-\frac{n}{\xi}P - F'\right)\sin(n\theta) \tag{24}$$

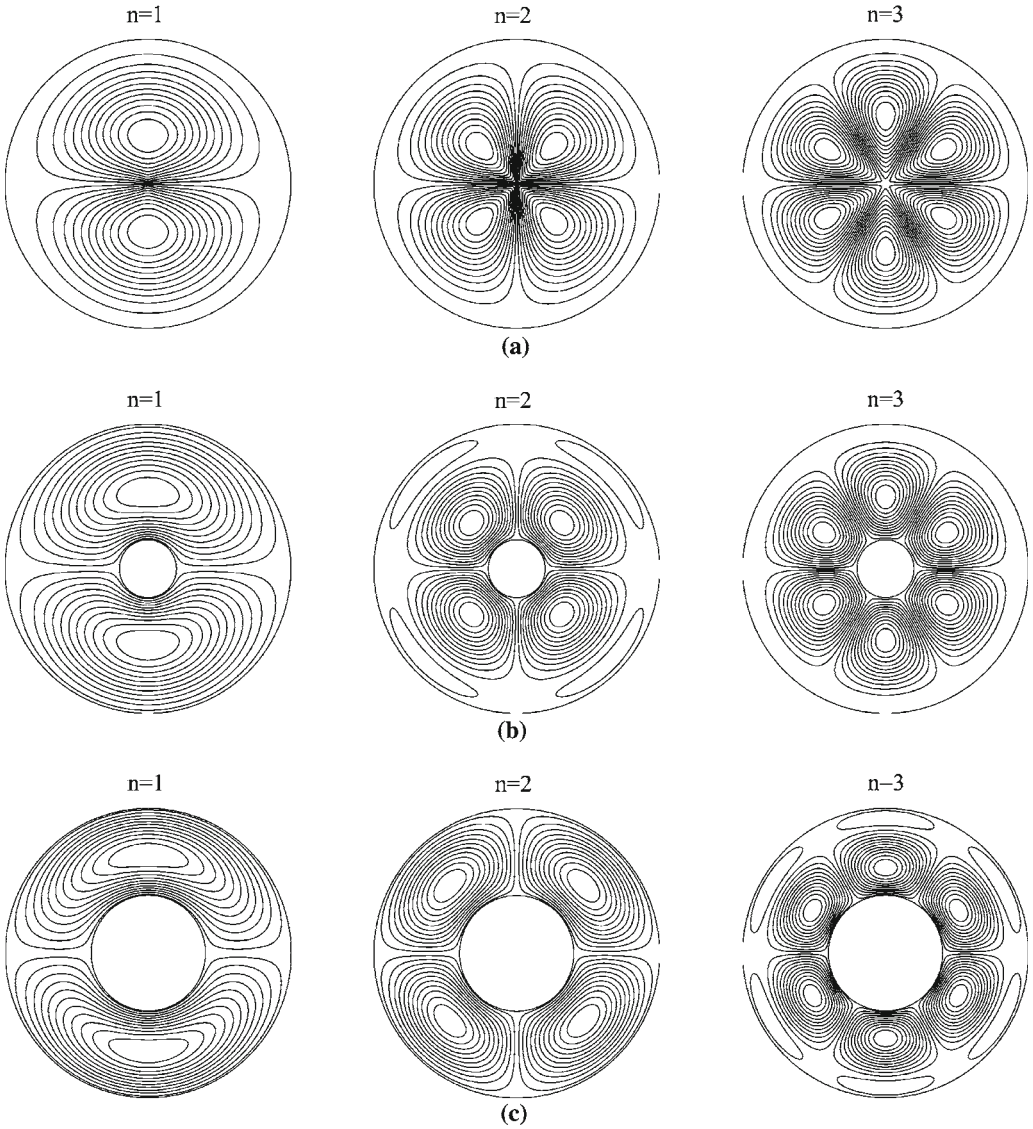

Fig. 3 Circumferential mode shapes distribution of Clamped-clamped boundary condition for n = 1, 2, 3 and **a** $\eta = 0$, **b** $\eta = 0.2$, **c** $\eta = 0.4$ corresponding to Table 2

Substituting P and F in above formulation leads to the following equations:

$$\widehat{u} = \frac{1}{R}\left\{\begin{array}{l} c_1\left[\frac{\beta-1}{2\beta}\xi^{-\frac{\beta+1}{2\beta}}J_m\left(\frac{\Omega\xi}{\sqrt{\beta}}\right)+\xi^{\frac{\beta-1}{2\beta}}\frac{d}{d\xi}\left(J_m\left(\frac{\Omega\xi}{\sqrt{\beta}}\right)\right)\right]+c_2\left[\frac{\beta-1}{2\beta}\xi^{-\frac{\beta+1}{2\beta}}Y_m\left(\frac{\Omega\xi}{\sqrt{\beta}}\right)+\xi^{\frac{\beta-1}{2\beta}}\frac{d}{d\xi}\left(Y_m\left(\frac{\Omega\xi}{\sqrt{\beta}}\right)\right)\right] \\ +d_1\left[n\xi^{-\frac{\mu+\lambda}{2\mu}}J_z\left(\frac{\Omega\xi}{\sqrt{\mu\sqrt{g}}}\right)\right]+d_2\left[n\xi^{-\frac{\mu+\lambda}{2\mu}}Y_z\left(\frac{\Omega\xi}{\sqrt{\mu\sqrt{g}}}\right)\right] \end{array}\right\} \tag{25}$$

$$\widehat{v} = -\frac{1}{R}\left\{\begin{array}{l} c_1 n\xi^{-\frac{\beta+1}{2\beta}}J_m\left(\frac{\Omega\xi}{\sqrt{\beta}}\right)+c_2 n\xi^{-\frac{\beta+1}{2\beta}}Y_m\left(\frac{\Omega\xi}{\sqrt{\beta}}\right)+d_1\left[\frac{\mu-\lambda}{2\mu}\xi^{-\frac{\mu+\lambda}{2\mu}}J_z\left(\frac{\Omega\xi}{\sqrt{\mu\sqrt{g}}}\right)+\xi^{\frac{\mu-\lambda}{2\mu}}\frac{d}{d\xi}J_z\left(\frac{\Omega\xi}{\sqrt{\mu\sqrt{g}}}\right)\right] \\ +d_2\left[\frac{\mu-\lambda}{2\mu}\xi^{-\frac{\mu+\lambda}{2\mu}}Y_z\left(\frac{\Omega\xi}{\sqrt{\mu\sqrt{g}}}\right)+\xi^{\frac{\mu-\lambda}{2\mu}}\frac{d}{d\xi}Y_z\left(\frac{\Omega\xi}{\sqrt{\mu\sqrt{g}}}\right)\right] \end{array}\right\} \tag{26}$$

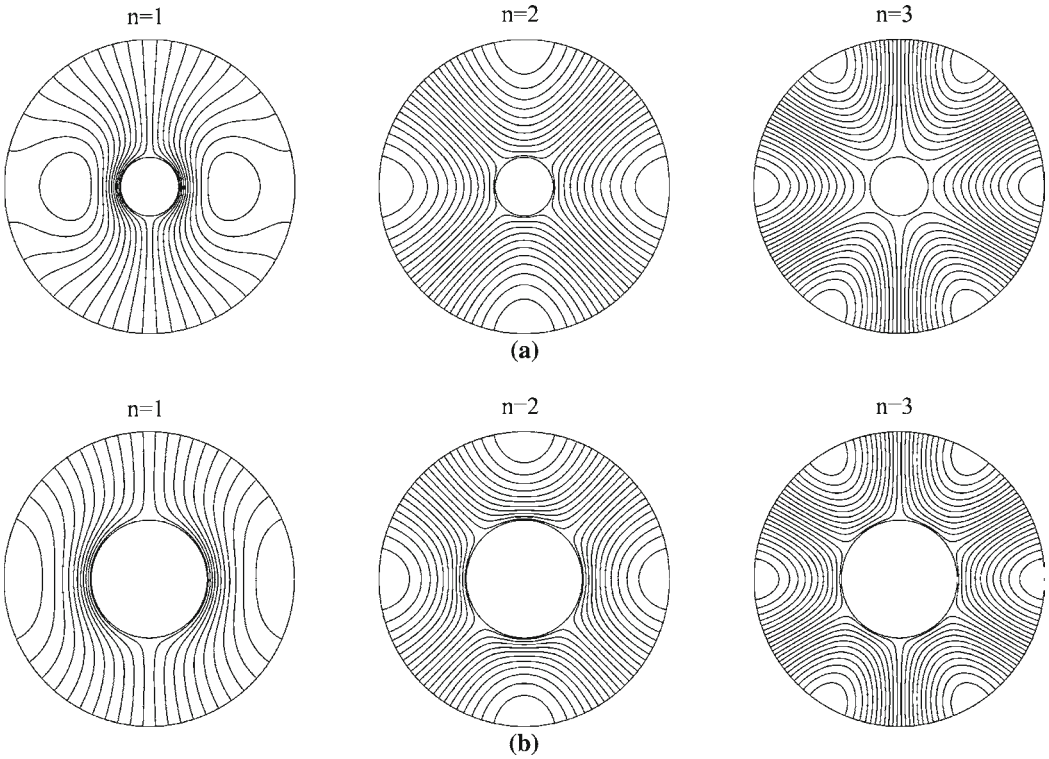

Fig. 4 Radial mode shapes distribution of Clamped-Free boundary condition for $n = 1, 2, 3$ and **a** $\eta = 0.2$, **b** $\eta = 0.4$ corresponding to Table 3

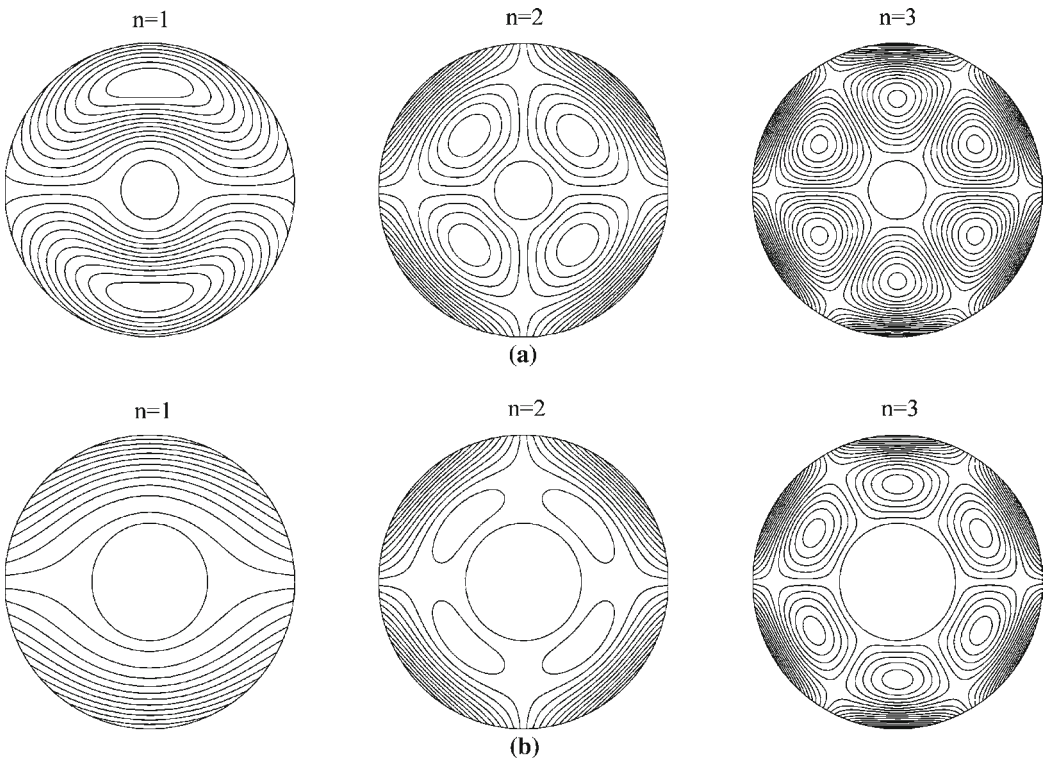

Fig. 5 Circumferential mode shapes distribution of Clamped-free boundary condition for $n = 1, 2, 3$ and **a** $\eta = 0.2$, **b** $\eta = 0.4$ corresponding to Table 3

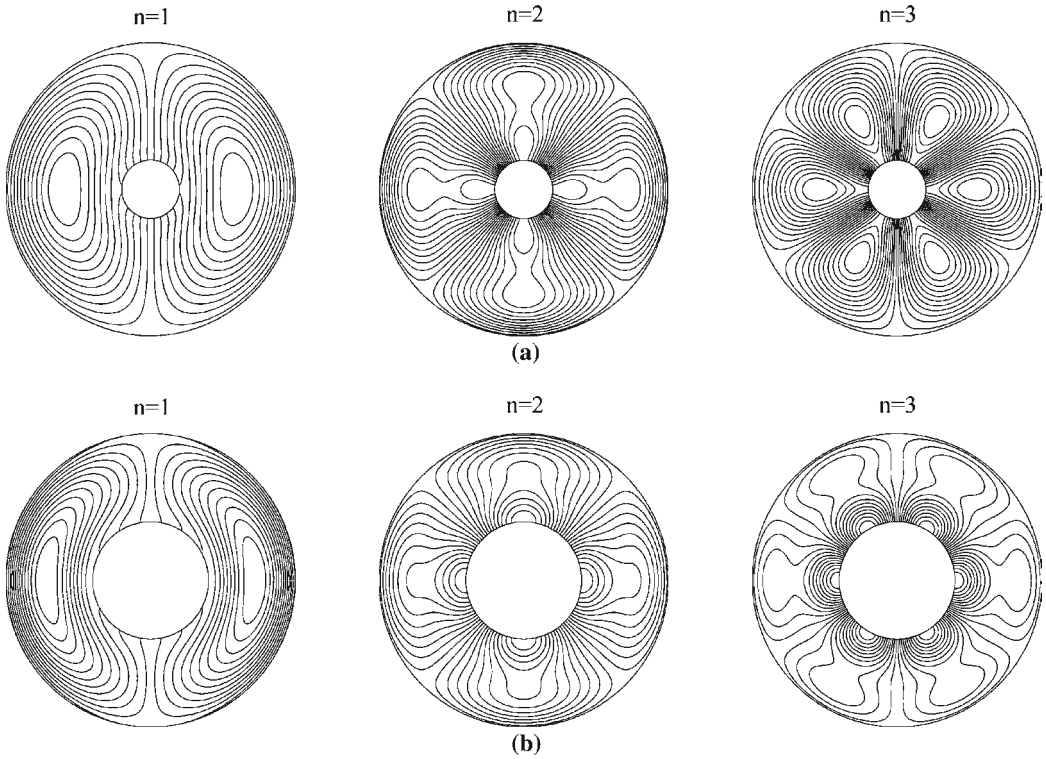

Fig. 6 Radial mode shapes distribution of Free-clamped boundary condition for n = 1, 2, 3 and **a** $\eta = 0.2$, **b** $\eta = 0.4$ corresponding to Table 4

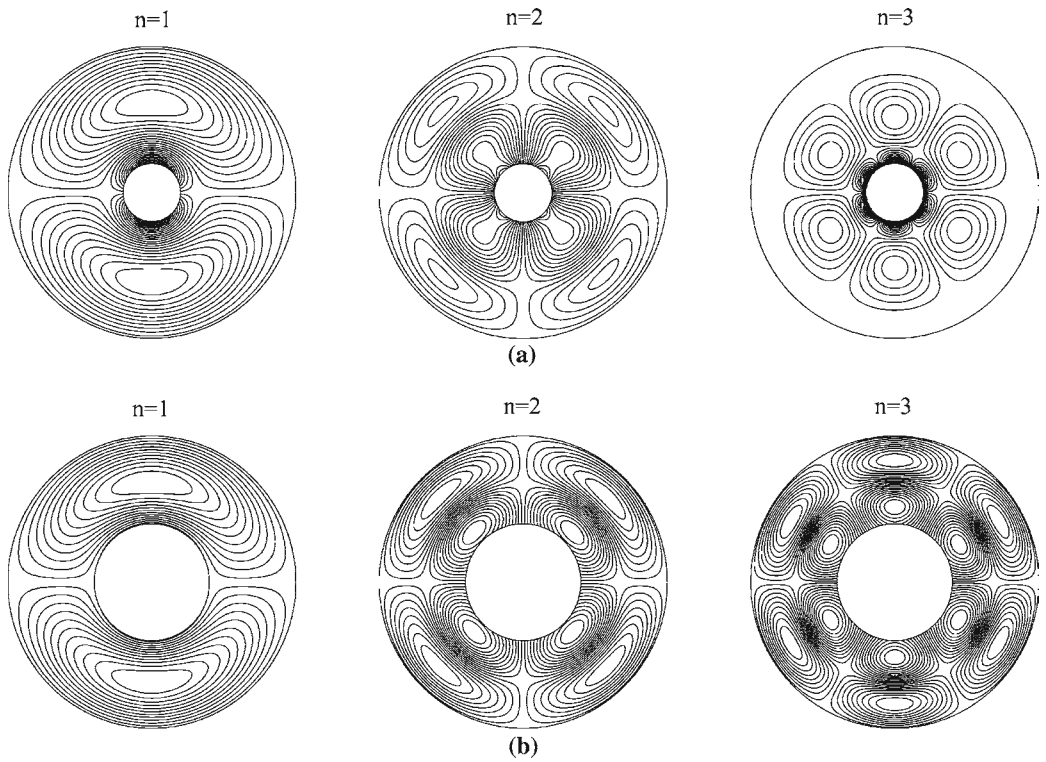

Fig. 7 Circumferential mode shapes distribution of Free-clamped boundary condition for n = 1, 2, 3 and **a** $\eta = 0.2$, **b** $\eta = 0.4$ corresponding to Table 4

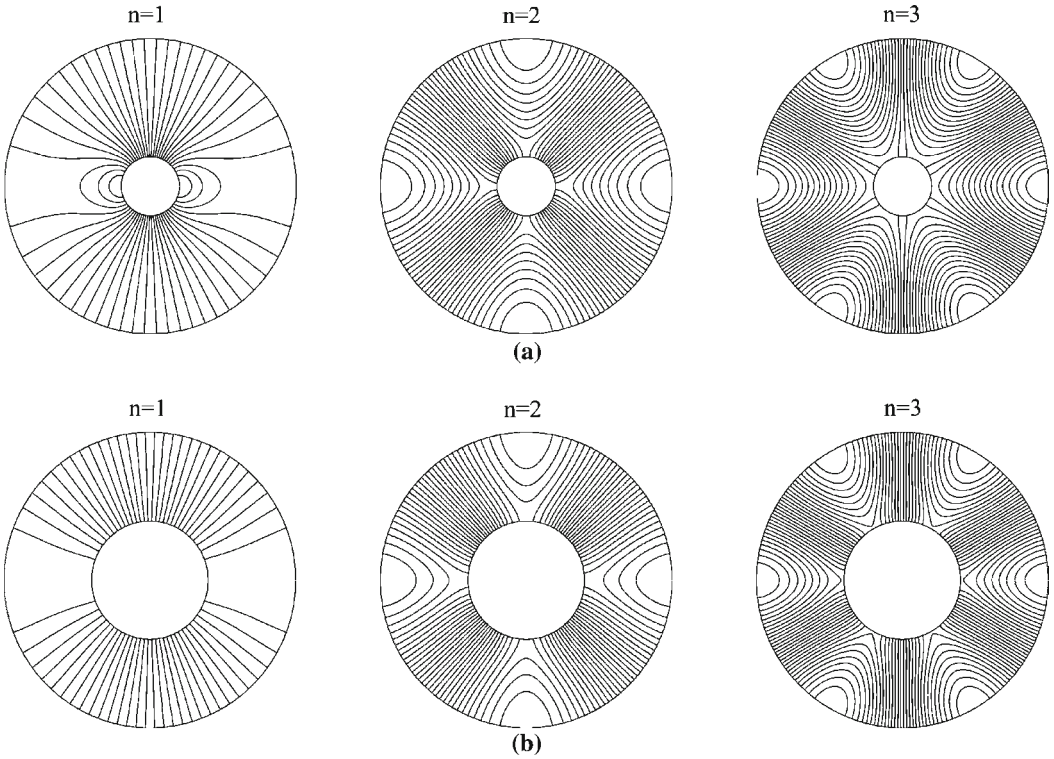

Fig. 8 Radial mode shapes distribution of Free-free boundary condition for n = 1, 2, 3 and **a** $\eta = 0.2$, **b** $\eta = 0.4$ corresponding to Table 5

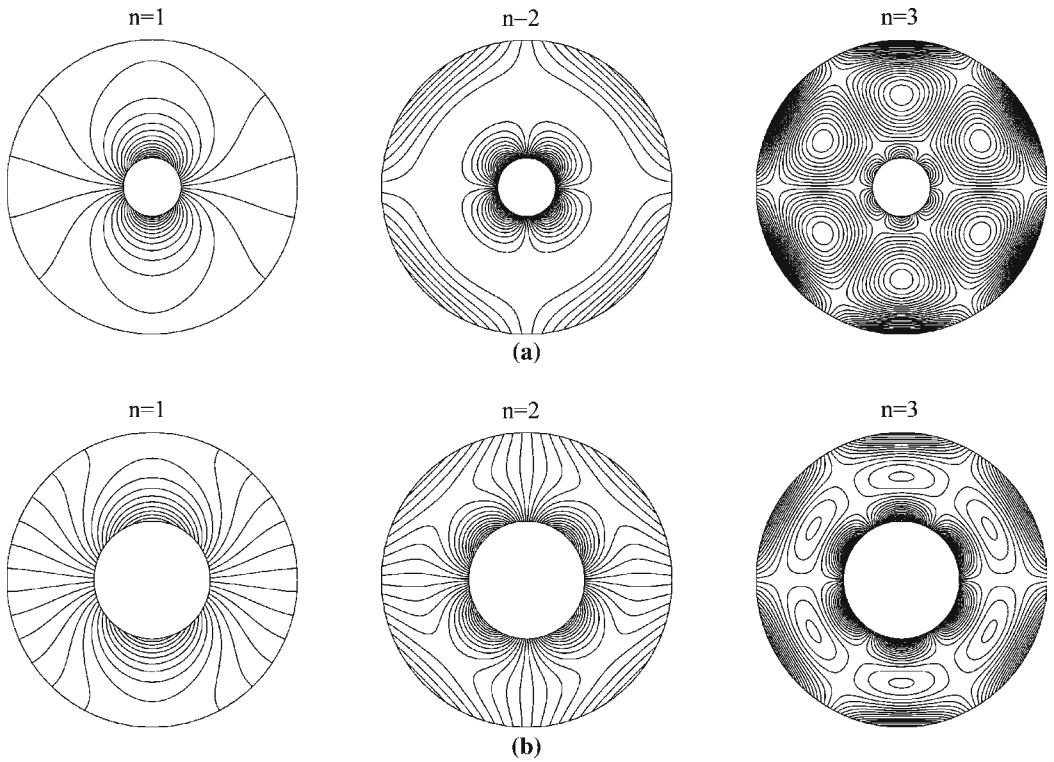

Fig. 9 Circumferential mode shapes distribution of Free-free boundary condition for n = 1, 2, 3 and **a** $\eta = 0.2$, **b** $\eta = 0.4$ corresponding to Table 5

Table 6 Material properties

Material	E_r (Gpa)	E_θ (Gpa)	G (Gpa)	ν_r	ν_θ	ρ (kg/m^3)
Polycarbonate	2.2	2.2	0.846	0.3	0.295	1.220
GFRP (E-glass/Epoxy)	38.6	8.27	4.14	0.26	0.056	1.800
CFRP (T300/N5208)	181.0	10.3	7.17	0.28	0.016	1.600

Table 7 Non-dimensional first natural frequencies (Ω) of in-plane vibration for clamped-clamped conditions and orthotropic materials in Table 6

Material	Radial ratio	Clamped-clamped		Clamped-free		Free-clamped		Free-free	
		Present study	FEM model	Present study	FEM model	Present study	FEM model	Present study	FEM model
Polycarbonate	0.2	1.402	1.388	0.928	0.919	2.107	2.104	1.661	1.652
	0.4	2.411	2.393	1.297	1.281	2.601	2.517	1.700	1.683
GFRP (E-glass/Epoxy)	0.2	0.763	0.747	0.0312	0.0308	0.1501	0.1498	0.0930	0.0923
	0.4	1.296	1.286	0.0725	0.0720	0.0773	0.0756	0.0579	0.0578
CFRP (T300/N5208)	0.2	0.451	0.439	0.0192	0.0188	0.0919	0.0908	0.0529	0.0524
	0.4	0.730	0.722	0.0451	0.0440	0.0449	0.0442	0.0320	0.0315

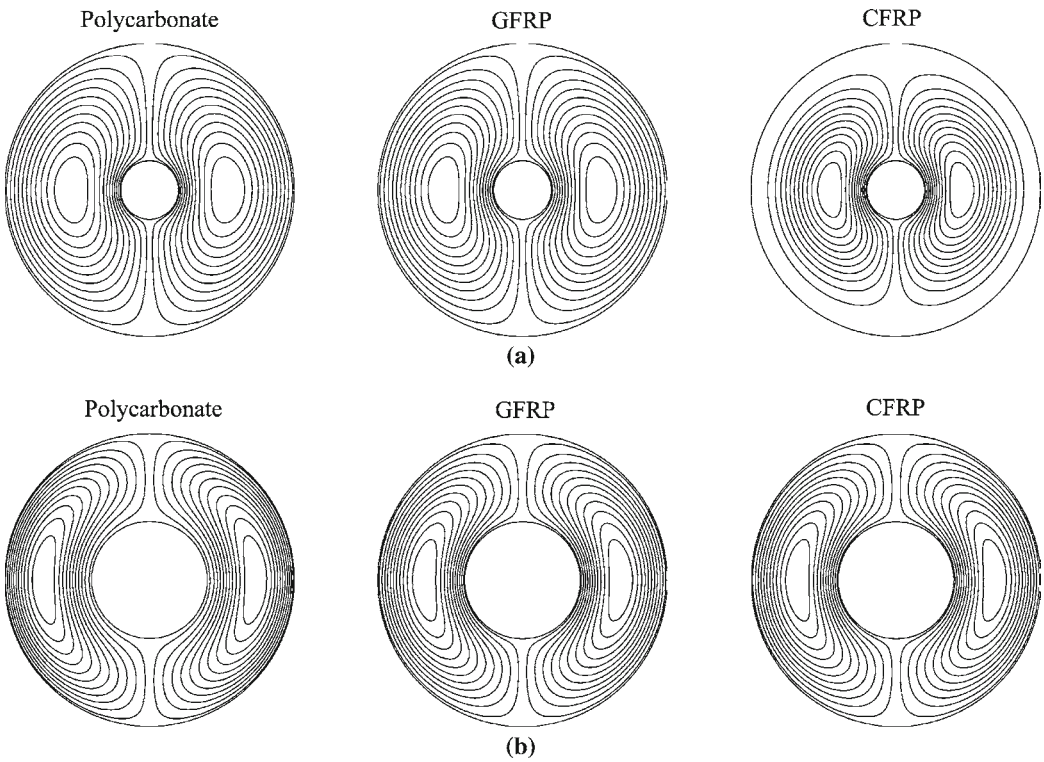

Fig. 10 Radial mode shapes distribution of Clamped-clamped boundary condition for **a** $\eta = 0.2$, **b** $\eta = 0.4$ corresponding to Table 7

where non-dimensional parameter $\eta = \frac{R_0}{R}$ is introduced. Application of the general boundary conditions, presented in Table 1, and finding the evident solution, yields the frequency equation corresponding to those boundary conditions. The numerical solution of the frequency equations for a given n produces the natural frequencies.

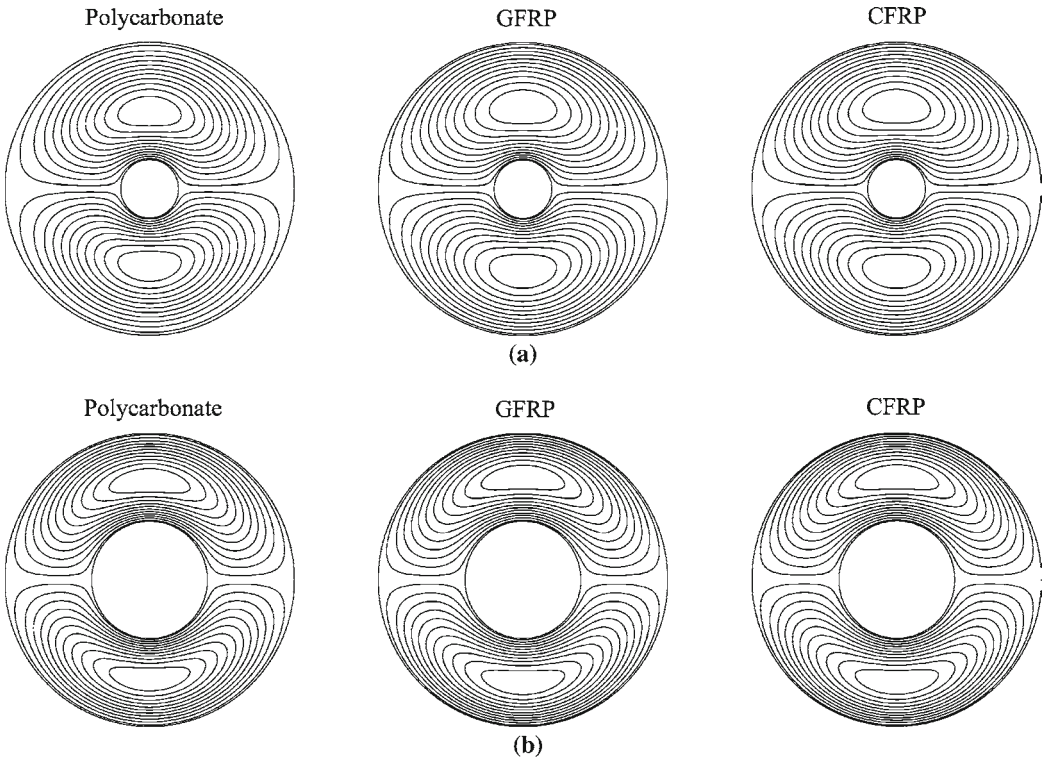

Fig. 11 Circumferential mode shapes distribution of Clamped-clamped boundary condition for **a** $\eta = 0.2$, **b** $\eta = 0.4$ corresponding to Table 7

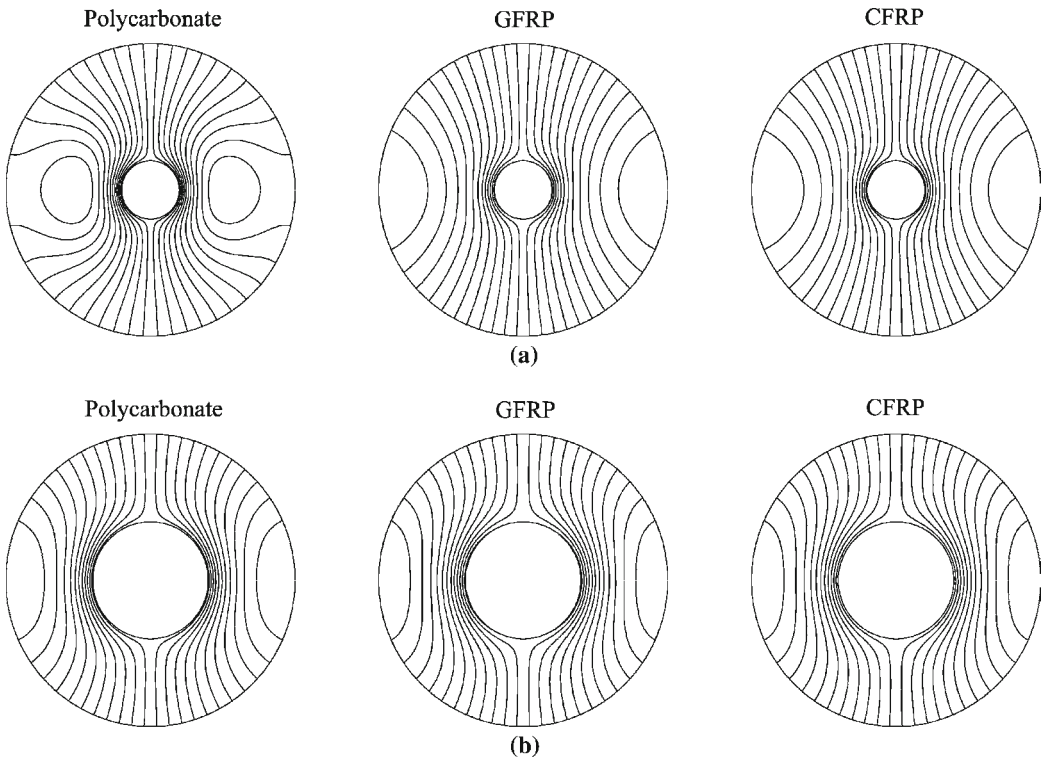

Fig. 12 Radial mode shapes distribution of Clamped-free boundary condition for **a** $\eta = 0.2$, **b** $\eta = 0.4$ corresponding to Table 7

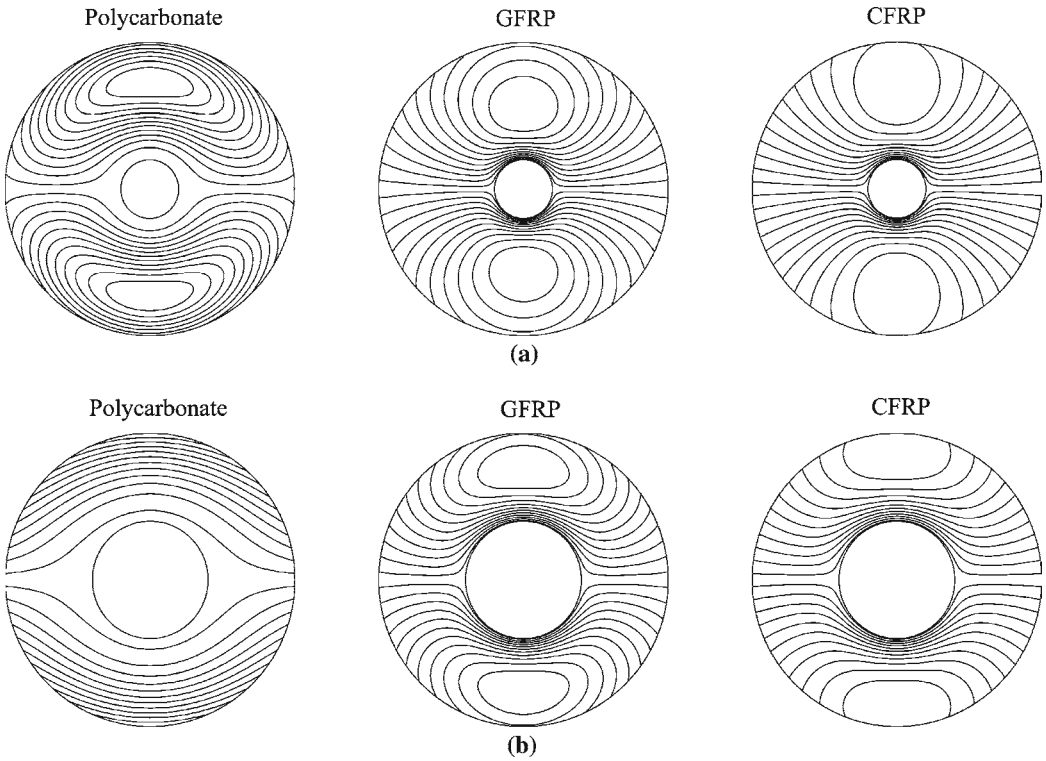

Fig. 13 Circumferential mode shapes distribution of Clamped-free boundary condition for **a** $\eta = 0.2$, **b** $\eta = 0.4$ corresponding to Table 7

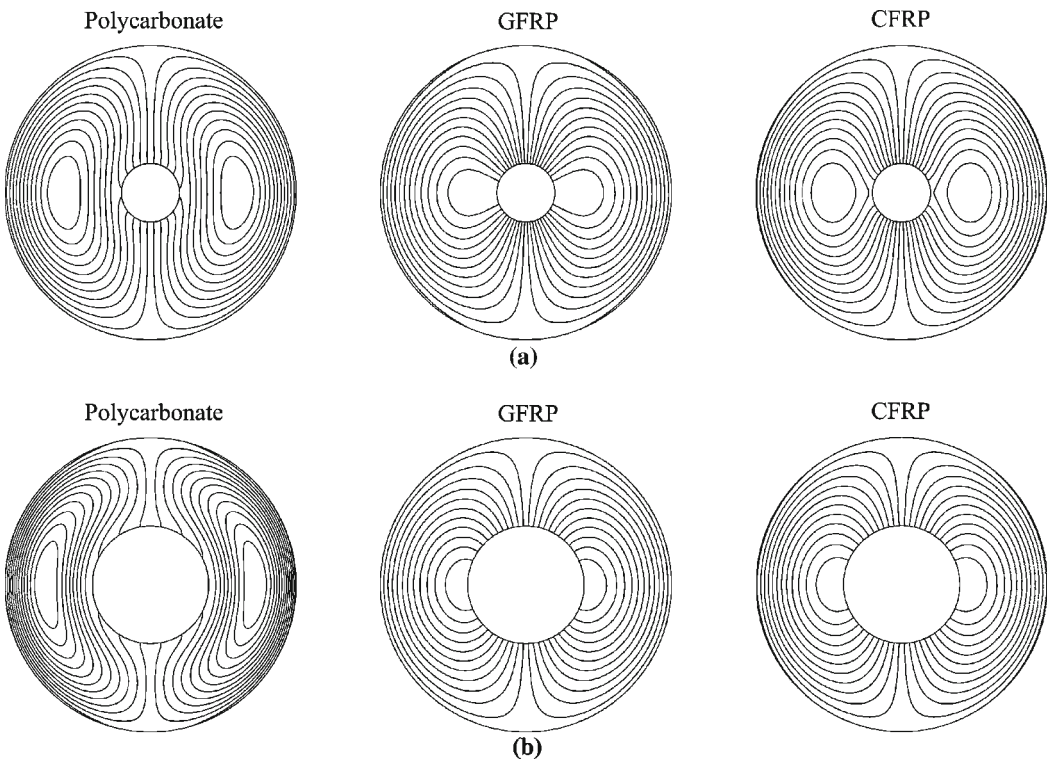

Fig. 14 Radial mode shapes distribution of Free-clamped boundary condition for **a** $\eta = 0.2$, **b** $\eta = 0.4$ corresponding to Table 7

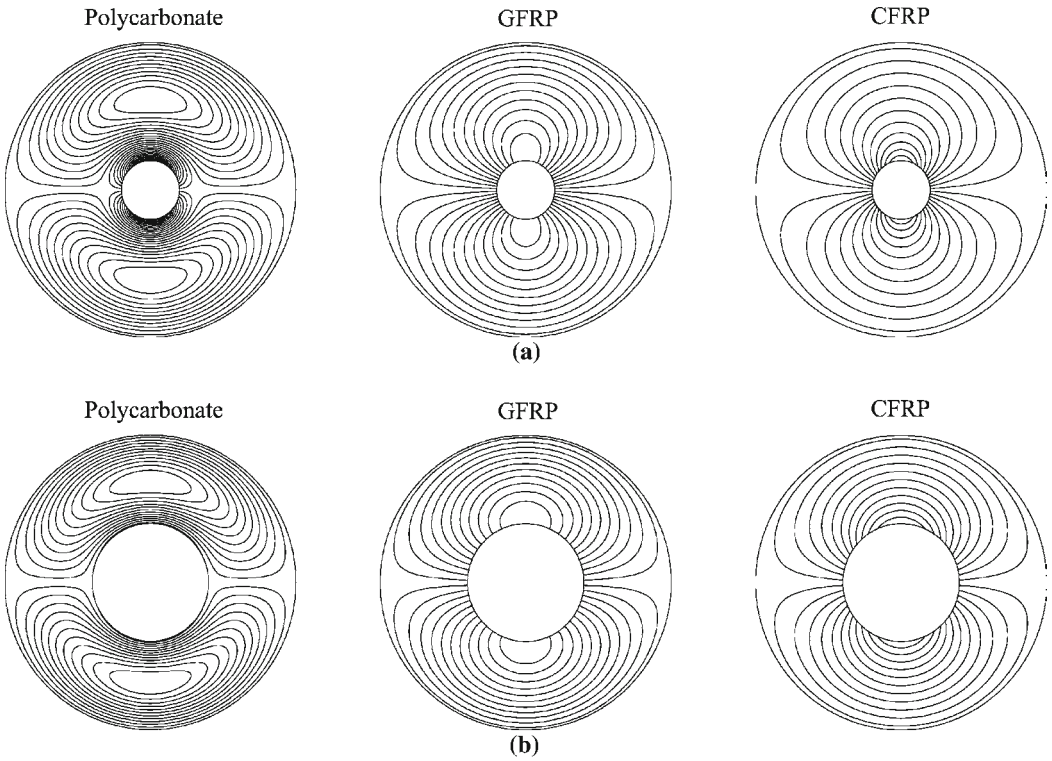

Fig. 15 Circumferential mode shapes distribution of Free-clamped boundary condition for **a** $\eta = 0.2$, **b** $\eta = 0.4$ corresponding to Table 7

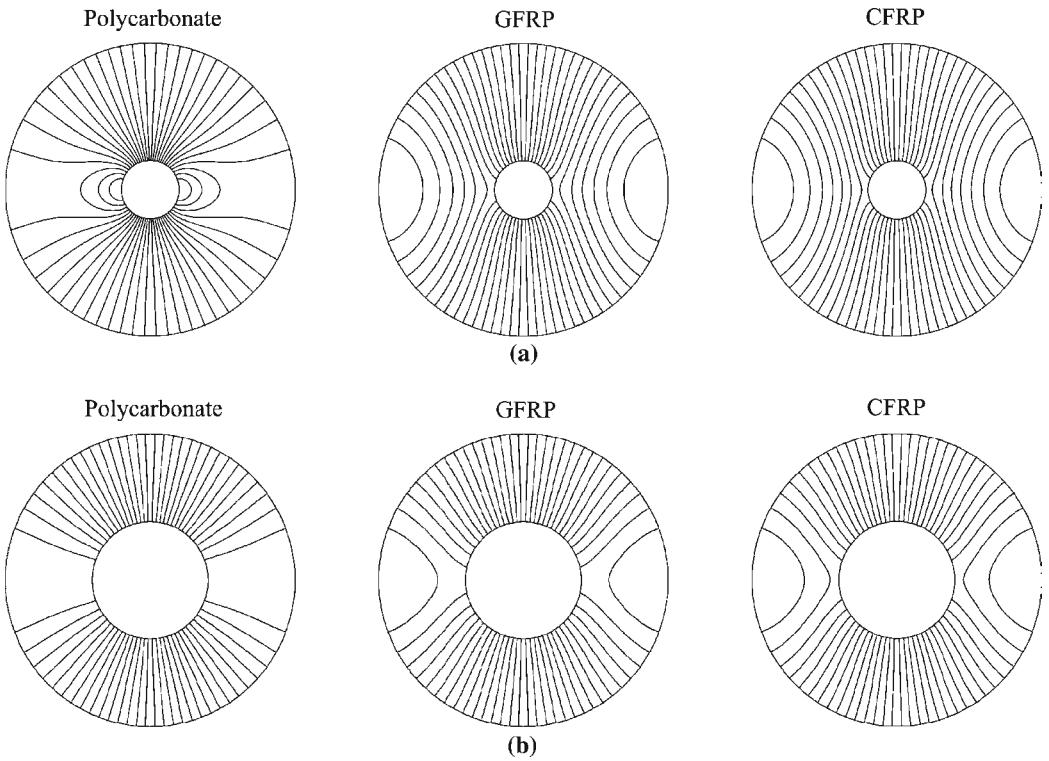

Fig. 16 Radial mode shapes distribution of Free-free boundary condition for **a** $\eta = 0.2$, **b** $\eta = 0.4$ corresponding to Table 7

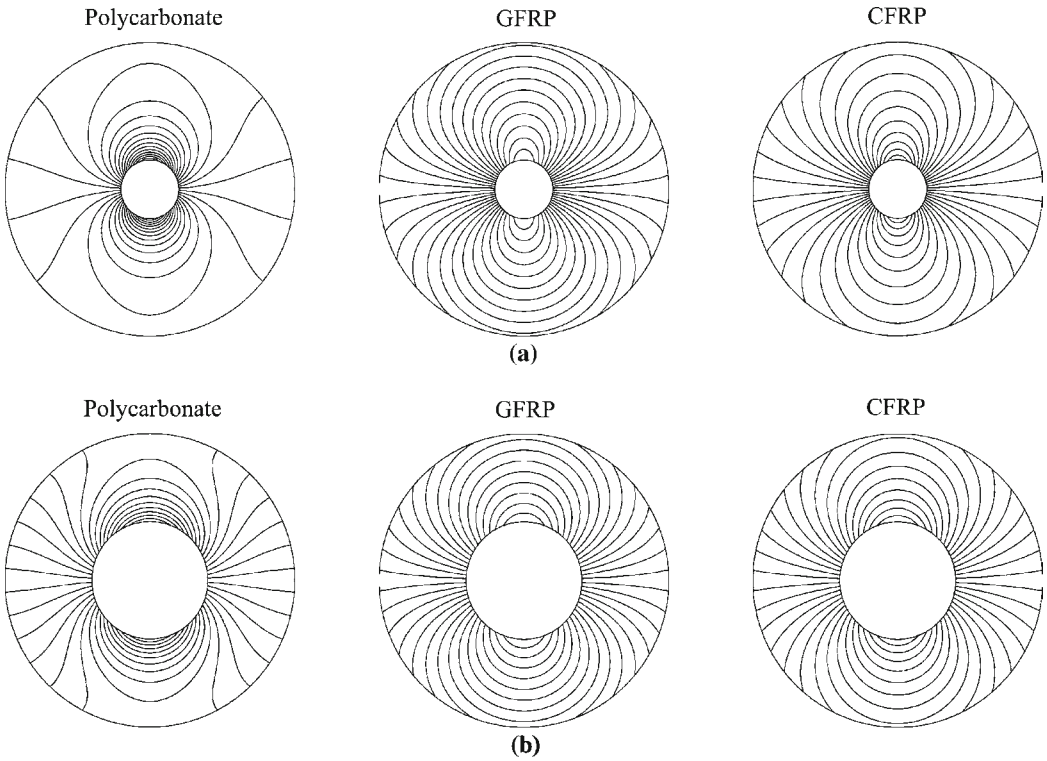

Fig. 17 Circumferential mode shapes distribution of Free-free boundary condition for **a** $\eta = 0.2$, **b** $\eta = 0.4$ corresponding to Table 7

3 Results

The solution of the frequency equations is obtained using a MATLAB program and the first in-plane dimensionless frequencies for isotropic and orthotropic materials are tabulated. The results are obtained for general boundary conditions presented in Table 1. Tables 2, 3, 4 and 5 present the first dimensionless in-plane frequencies for an isotropic material with $\nu = 0.3$ for clamped-clamped, Clamped-free, free-Clamped and free-free boundary conditions, respectively. These frequencies are presented for different radial ratios. Maximum difference among the present results and other studies is about 5%; it occurs for a solid disk and for $n = 1$. Radial and circumferential distribution of the mode shapes corresponding to each boundary condition are depicted in Figs. 2, 3, 4, 5, 6, 7, 8 and 9.

Properties of three materials which selected to calculate the first natural in-plane frequency of orthotropic materials are shown in Table 6 [12]. To validate the analytical results, the first in-plane natural frequency is also computed using the finite element method. The plate is modeled using ABAQUS V6.8-1 and all results are calculated for $n = 1$. In these models, CPS4R and CPS3 elements are used, 540 elements and 541 nodes are applied for solid disk for example.

Table 7 lists these results. Maximum difference among the results of present study and FEM model is about 2.8 percent. Figures 10, 11, 12, 13, 14, 15, 16 and 17 show radial and circumferential distribution of mode shapes corresponding to Table 7.

The obtained results by present frequency equations are in agreement with those of the other studies and FEM models. Therefore, the proposed frequency equations could be used to calculate the first natural in-plane frequency of isotropic and orthotropic circular annular plates.

4 Summary and conclusions

Orthotropic circular annular plate natural in-plane frequency equations were derived by using equations of motion in the cylindrical coordinate. The equations of motion are coupled and therefore, Helmholtz decomposition was used to change them to uncouple equations. Then the frequency equations for general boundary

conditions of circular annular plate were derived. The first natural in-plane frequency for isotropic and orthotropic materials was computed through numerical examples. The presented results were validated with the previous reports and the finite element model. This verification showed that the proposed method is accurate for calculating the natural in-plane frequencies of circular annular plates.

References

1. Irie, T., Yamada, G., Muramoto, Y.: Natural frequencies of in-plane vibration of annular plates. J. Sound Vib. **97**, 171–175 (1984)
2. Ambati, G., Bell, J.F.W., Sharp, J.C.K.: In-plane vibrations of annular rings. J. Sound Vib. **47**, 415–432 (1976)
3. Farag, N.H., Pan, J.: Modal characteristics of in-plane vibration of circular plates clamped at the outer edge. J. Acous. Soc. Am. **113**, 1935–1946 (2003)
4. Holland, R.: Numerical studies of elastic-disk contour modes lacking axial symmetry. J. Acous. Soc. Am. **40**, 1051–1057 (1966)
5. Kane, T.R., Mindlin, R.D.: High-frequency extensional vibrations of plates. J. Appl. Mech. **23**, 277–283 (1956)
6. Chen, S.S.H., Liu, T.M.: Extensional vibration of thin plates of various shapes. J. Acous. Soc. Am. **58**(4), 828–831 (1975)
7. Love, A.E.H.: A Treatise on the Mathematical Theory of Elasticity. 4th edn. Dover, New York (1944)
8. Bashmal, S., Bhat, R., Rakheja, S.: In-plane free vibration of circular annular disks. J. Sound Vib. **322**, 216–226 (2009)
9. Chen, J.S., Jhu, J.L.: On the in-plane vibration and stability of a spinning annular disk. J. Sound Vib. **195**(4), 585–593 (1996)
10. Park, C.: Frequency equation for the in-plane vibration of a clamped circular plate. J. Sound Vib. **313**, 325–333 (2008)
11. Michael, W., Rubin, D., Krempl, E.: Introduction to Continuum Mechanics. 3rd edn. Pergamo, The united states of America (1993)
12. Koo, K.N.: Vibration analysis and critical speeds of polar orthotropic annular disks in rotation. Compos. Struct. **76**, 67–72 (2006)
13. Doyle, J.F.: Wave Propagation in Structures. 2nd edn. Springer, New York (1997)
14. Achenbach, J.D.: Wave Propagation in Elastic Solid. North-Holland Publishing, Amsterdam (1973)